Separation and Purification Technology 354 (2025) 128657

Contents lists available at ScienceDirect

Separation and Purification Technology

journal homepage: www.elsevier.com/locate/seppur

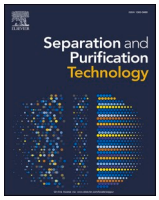

Porous alumina-supported lithium aluminum titanium phosphate membrane for lithium extraction using the electrodialysis process

Umma Habiba [a,*], Tawsif Ahmed Siddique [b], Islam Md Rizwanul Fattah [c], Shabin Mohammed [a], Edward Attenborough [a], Quan Lai [d], Zhouyou Wang [a]

[a] Department of Chemical and Biological Engineering, Faculty of Engineering, Monash University, Clayton 3800, Victoria, Australia
[b] Chemical and Environmental Engineering, School of Engineering, RMIT University, Melbourne, VIC 3000, Australia
[c] Centre for Technology in Water and Wastewater (CTWW), School of Civil and Environmental Engineering, Faculty of Engineering and IT, University of Technology Sydney, Ultimo, NSW 2007, Australia
[d] Department of Mechanical and Aerospace Engineering, Faculty of Engineering, Monash University, Clayton 3800, Victoria, Australia

ARTICLE INFO

Editor: B. Van der Bruggen

Keywords:
Electrodialysis
Lithium
Lithium aluminum titanium phosphate (LATP)
Electrolyte membrane

ABSTRACT

Inorganic membranes that possess lithium ionic conductivity exhibit considerable potential as a viable option for the targeted extraction of lithium from brine sources. However, the practical implementation of ceramic anisotropic thin film membranes for lithium-ion extraction presents ongoing challenges due to the scarcity of suitable membrane materials and complex fabrication techniques. This research proposes an innovative approach to address this issue by employing a battery material, a lithium-ion conducting electrolyte, to produce a membrane that selectively permits the passage of lithium ions. A scalable approach was employed to fabricate an asymmetric lithium aluminum titanium phosphate (LATP) membrane by utilizing a citric acid-assisted sol–gel coating method on a porous alumina substrate and subsequent sintering. A continuous and compact LATP membrane with an approximate thickness of 14.32 ± 1.36 μm was successfully deposited onto the porous support through the dip coating technique. The lithium-ion permeation was checked using the electrodialysis system from a feed solution containing Li^+ coexisting with Na^+ and Mg^{2+}. A high lithium flux of 215 mmol/h/m^2 with a Li^+/Mg^{2+} selectivity of 33 was produced when 2 V of voltage was applied to the 1.65 cm2 ionic conductor anisotropic membrane containing a mixed alkaline solution containing lithium chloride, sodium chloride, and magnesium chloride at the feed solution. These findings underscore the potential for producing lithium-selective membranes using electrolyte materials.

1. Introduction

Lithium (Li) is one of the key materials for Li-ion and lithium–sulfur batteries (Li–S battery), which is a type of rechargeable battery [1]. The escalating demand for Li in the electric vehicle industry has led to a significant rise in its price. Consequently, an urgent requirement is to augment Li production to meet this exponential demand [2]. Abundant reserves of Li can be found in Li salt lake brines and seawater. China, Bolivia, Argentina, and Chile are notable regions where significant quantities of Li are extracted from brine sources [3,4]. Various types of multistage processes are employed for Li extraction, with the evaporation-precipitation method being the predominant approach [5]. Alternative methods of extraction are taken into account, as the solar evaporation method necessitates a time frame of 10–20 months following the brine's extraction to the surface [4].

In recent years, significant endeavors have been undertaken to enhance the Li recovery process and develop alternative methods that do not rely on evaporation [6,7]. The utilization of membrane technology in Li extraction presents a substantial opportunity to reduce operational expenses through the simplification of extraction methods. While reverse osmosis and nanofiltration are commonly employed pressure-driven membrane processes for brine treatment [8], these membranes face certain constraints, including fouling, inadequate Li selectivity, and low recovery rates [8,9]. Consequently, electrodriven processes have garnered significant interest as an alternative approach for Li extraction from brine-based sources [10].

Electrodialysis is an electro-driven separation technology in which ions are transported through a permeable membrane by applying a

* Corresponding author.
E-mail address: habiba062012@gmail.com (U. Habiba).

https://doi.org/10.1016/j.seppur.2024.128657
Received 13 January 2024; Received in revised form 30 June 2024; Accepted 1 July 2024
Available online 2 July 2024

voltage difference [11]. The experimental setup involves an electrodialysis stack, wherein cation exchange and anion exchange membranes are arranged alternately [12,13]. Anion exchange membranes are membranes with functional groups that are positively charged. These membranes reject cations and permit the passage of anions. However, a cation exchange membrane's function is to selectively allow cations to pass through it from the anode to the cathode [14,15].

The electrodialysis process holds potential as a technique for extracting Li from aqueous solutions using suitable membranes that allow selective passage of Li. Consequently, it is critical to identify an appropriate membrane material for this process. Fortunately, ongoing research and development on Li-conductive materials and membranes, including ceramics, polymers, hybrids, and liquid electrolytes, primarily for battery applications [16], offer possibilities for implementation in membrane separation processes. Ceramic electrolytes, for instance, ensure high safety and stability. They can be categorized based on their crystal structure, such as LISICON, NASICON, perovskite, garnet-type, Lithium nitride (Li_3N)-type, LiPON-type, anti-perovskite-type, argyrodite-type, and others [17]. Among these, NASICON-type Lithium aluminum titanium phosphate (LATP) and Lithium aluminum germanium phosphate (LAGP), perovskite-type Lithium lanthanum titanate (LLTO) and garnet-type cubic Lithium lanthanum zirconium oxide (LLZO) have promising ion conductivity at room temperature [17,18]. However, while LLZO shows great potential due to its high electrochemical window, challenges remain in achieving a stable cubic phase and addressing its moisture sensitivity [19]. Additionally, LLZO necessitates high temperatures for calcination and sintering, thereby increasing the likelihood of impurity formation through reactions with the ceramic substrate [20–22]. Consequently, fabricating thin film composite structures from LLZO is difficult. Furthermore, LAGP is impractical for large-scale applications due to the high cost of germanium, an essential component.

Lithium aluminum titanium phosphate (LATP), a ceramic material with high Li conductivity, is regarded as a superionic material due to its enhanced ion transport capability at room temperature (ϵ 10^{-3} S m^{-1}) [23]. Integrating LATP into Li-selective membranes holds promise for various applications. However, achieving a highly pure LATP phase is crucial to obtain the desired ion transport properties [24]. Unfortunately, obtaining a pure LATP phase is challenging since it is often accompanied by the presence of the impurity phase $AlPO_4$ during the calcination process, typically occurring within the temperature range of 700–1200 °C [25].

The sol–gel method is highly regarded for its ability to easily obtain pure-phase nanoparticles by controlling process parameters [26]. Moreover, this method has been widely employed for the production of ceramic thin film membranes for many years [27–30]. Fortunately, there are modified approaches that have proven successful in creating thin films, with the Pechini process being particularly popular due to its simplicity and cost-effectiveness [31–35]. The deposition of thin membranes through the Pechini sol–gel route typically involves five steps: preparing a stable sol solution, coating the sol onto the substrate (whether porous or nonporous), drying, removing organic compounds through combustion, and densifying the film at high temperatures [36]. First, it is crucial to prepare a stable sol solution that prevents the precipitation of small particles. When depositing ceramic thin membranes onto a porous layer using the sol–gel method, a major challenge is to avoid solution infiltration into the pores. Solution infiltration can lead to surface film discontinuities and blockage of the substrate's pores. This impedes mass transport through the substrate and compromises the selectivity of the dense upper layer. Therefore, creating a stable and viscous sol is essential to prevent sol infiltration into the pores. Initially, Satoko et al. [16] reported the preparation of a viscous sol for making an ultrathin LATP film on a nonporous substrate using the Pechini method. However, this knowledge cannot be directly applied to the production of thin films on a porous support.

In this study, using the Pechini approach, a citric acid-assisted stable sol was prepared from titanium alkoxide and nitrate salt of Li and aluminum. The sol can be deposited on the substrate using spin coating and dip coating methods [24]. Although spin coating is preferable for creating thin films, dip coating was chosen in this case to deposit the LATP sol onto an alumina substrate, as it offers better coverage of the substrate's larger surface area. The Li permeability through the LATP thin film membrane was tested by electrodialysis. It was shown that the membrane structure played a crucial role in achieving a notable Li flux of 215 mmol/h/m^2, coupled with a Li_+/Mg^{2+} selectivity of 33. These results highlight the promising prospect of developing Li-selective membranes utilizing electrolyte materials.

2. Experimental details

2.1. Materials

Ammonium phosphate dibasic ($(NH_4)_2HPO_4$), lithium nitrate ($LiNO_3$), aluminum nitrate nonahydrate (Al $(NO_3)_3{\cdot}9H_2O$), titanium butoxide ($Ti(C_4H_9O)_4$), polyvinyl alcohol (PVA, Mw = 89,000–98,000), sodium chloride (NaCl), lithium chloride (LiCl), magnesium chloride ($MgCl_2$), citric acid and ethylene glycol were purchased from Sigma Aldrich. Alumina powder (2–3 μm) was purchased from Hangzhou Jikang New Material Co., Ltd, and anion exchange membrane (AEM) SELEMION^{TM} AMVN, 100 μm, was purchased from AGC Company, Japan.

2.2. Preparation of LATP sol and LATP nanoparticles

While sol–gel deposition represents a powder-free technique, it is essential to synthesize LATP powder from the sol to enhance the process parameters and achieve a purer phase of LATP and a finer grain size. Furthermore, comprehension of the microstructure of LATP is necessary to effectively optimize the parameters during the densification of the thin film [17]. Consequently, the sol solution containing LATP was subjected to calcination at various temperatures, and subsequent analysis was conducted to examine the morphology and microstructure.

The precursors used for LATP sol preparation were $LiNO_3$, Al $(NO_3)_3{\cdot}9H_2O$, $(NH_4)_2HPO_4$ and $Ti(C_4H_9O)_4$). First, 100 ml of 0.2 M citric acid aqueous solution was prepared in a Schott bottle (citric acid: metal ion, C/M = 4:1). Then, $Ti(C_4H_9O)_4$) was added to the solution at 80 °C. The solution was stirred until the $Ti(C_4H_9O)_4$) was dissolved completely. Next, $LiNO_3$, $Al(NO_3)_3{\cdot}9H_2O$, and $(NH_4)_2HPO_4$ were added and stirred until homogeneity of the solution was observed. Finally, ethylene glycol (citric acid: ethylene glycol = 1:1) was added to promote esterification and polymerization. The solution was subjected to overnight stirring until it reached a thick viscous consistency of 50 ml, which was deemed suitable for thin film production. Unstable sols can result in particle deposition, while insufficient viscosity can lead to sol infiltration into the porous substrate. Hence, the sol was monitored for several hours prior to the coating process. Variations were made in terms of the C/M ratio, final solution concentration, and stirring duration to achieve a stable sol. To investigate the LATP phase, a small quantity of the solution was placed in a petri dish and subjected to drying in an oven set at 170 °C. Once the gel was completely dried, it was ground into a fine powder. Subsequently, pyrolysis was carried out at a temperature of 500 °C for a duration of 2 h. Finally, the resulting powder underwent calcination within a temperature range spanning from 600 to 950 °C.

2.3. Preparation of alumina porous substrate

The porous alumina ceramic substrate was prepared using a uniaxial pressing method using a stainless steel die. Alumina powder (2–3 μm) was mixed with a few drops of 10 % PVA solution and paraffin oil using a mortar and pestle. A total of 2.5 g of mixed powder was pressed at 10 MPa in a stainless-steel mold. The prepared disc was sintered at 1250 °C for 3 h. After cooling, the disc was polished with sandpaper and

sonicated for a few seconds to remove the loosely packed powder.

2.4. Preparation of the LATP/alumina thin film membrane

The fabrication of the LATP membrane involved utilizing a dip coating technique [37], with the sol preparation as shown in Fig. 1. One face of the disc-shaped alumina substrate was immersed in the sol solution for a duration of 6 sec, followed by air drying under ambient conditions. Subsequently, the membrane underwent sintering for 10 h in a temperature range of 850–900 °C. The selection of the sintering temperature was based on an examination of the LATP phase's microstructure at different temperatures, which will be expounded upon in the subsequent section.

2.5. Characterizations

The morphology of the ceramic powder, membrane surface, and thickness were measured using a Scanning Electron Microscope (SEM), Nova NanoSEM 450 (FEI, USA). The crystallographic analysis was performed at room temperature in a 2θ range of 2–90° by a X-ray powder diffraction (XRD), Miniflex 600 (Rigaku, Japan). The crystallographic analysis of the LATP/alumina anisotropic membrane was performed with a Bruker XRD, D8. The membrane performance was measured by analyzing the concentration of the permeate solution at different times using an Agilent inductively coupled plasma mass spectrometer (ICP–MS).

2.6. Mechanical properties of the LATP/Alumina membrane

A micro-hardness tester (MATSUZAWA DVK-1S) was utilized to measure the hardness (H) of the ceramic membranes. The H of the membranes was evaluated using a load of 9.8 N (1 kgf) with a holding time of 20 s. Five indentations were made for each sample, and the mean HV was determined.

2.7. Ion permeation test

The electrodialysis technique was employed to evaluate the selectivity and ion permeation properties. The experimental setup for electrodialysis, encompassing the membrane stack and transmission channel, is depicted in the following diagram (Fig. S1a). Also, the physical representation of the experimental setup can be observed in Fig. S1b.

As shown in Fig. S1a, the electrodialysis setup mainly consists of three chambers: feed solution, concentrating solution, and electrolyte solution chambers. A 100 ppm solution of Li^+, Na^+, and Mg^{2+} was used as the feed, where Milli-Q water was the concentrating solution. Both electrode compartments were filled from the same electrolyte solution (300 ppm K_2SO_4) tank. Pumps were utilized in the experimental setup to ensure the circulation of the relevant solution within the chambers. The membrane stack consisted of two types of membranes: anion exchange membranes (AEMs) and lithium selective membranes (LISM). The AEMs were positioned adjacent to the electrolyte solution chamber to impede the flow of cations into the feed and concentrating chamber. The operational voltage was set at 2.0 V, and the pump rate was maintained at 3.5 rotations per minute (rpm). At the beginning and after five hours, the electrolyte chamber's pH values were 5.5 and 4.59, respectively. The solution's pH was not adjusted with the use of any chemical.

The ion flux was quantified by determining the concentration of ions transferred from the feed side to the permeate side across the membrane's effective area. The effective area of the membrane was 1.65 cm^2. The permeate solution was collected every hour and subjected to analysis using ICP–MS to measure the concentration of ions. Where necessary, the samples were diluted with 2.0 % aqueous nitric acid.

The ion flux was calculated using the following equation:

$$F = \frac{C_t - C_0}{A \times t} \quad (1)$$

Here, C_o and C_t are the initial and final mole concentrations of specific ions (ppm) present in the permeate compartment, respectively. A is the effective area of the membrane (cm^2), and t is the operation time (h).

The ion selectivity was calculated by using the following equation:

Li^+/Mg^{2+} and Li^+/Na^+ were calculated using Eqs. (2) and (3), respectively.

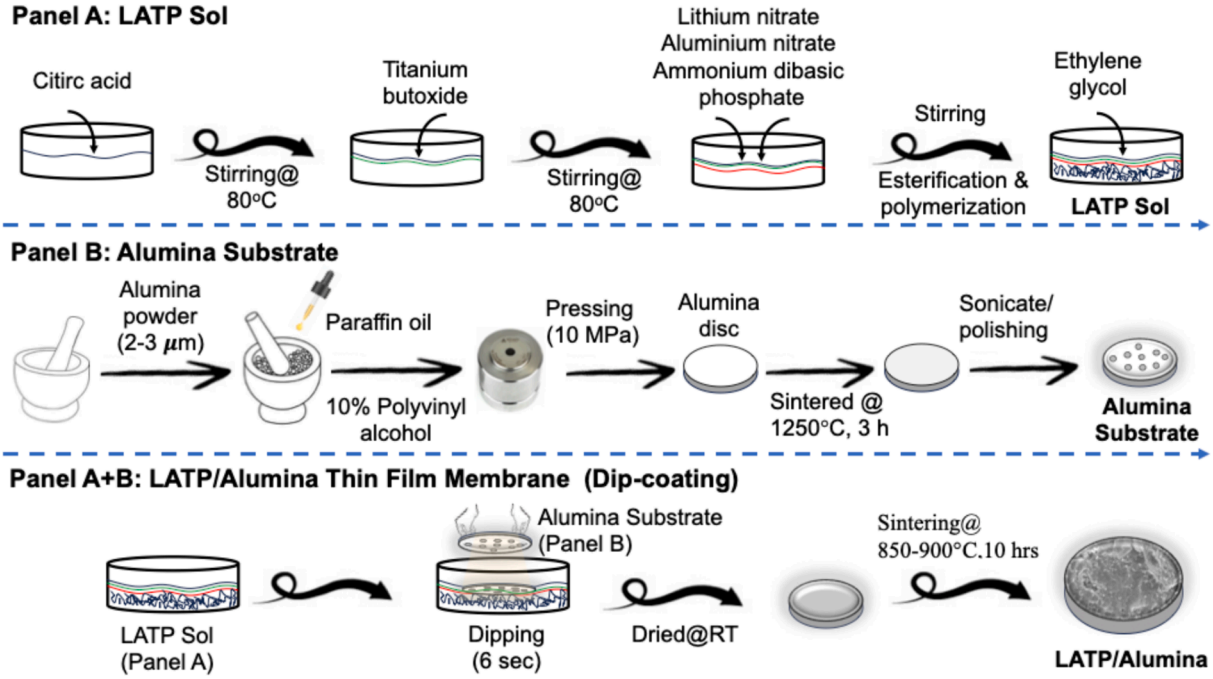

Fig. 1. Schematic illustration of LATP/alumina membrane fabrication procedure.

$$S_{Li/Mg} = \frac{C_{Li,permeate}}{C_{Li,feed}} / \frac{C_{Mg,permeate}}{C_{Mg,feed}} \quad (2)$$

$$S_{Li/Mg} = \frac{C_{Li,permeate}}{C_{Li,feed}} / \frac{C_{Mg,permeate}}{C_{Mg,feed}} \quad (3)$$

Here, $C_{Li,permeate}$, $C_{Li,feed}$, $C_{Mg,permeate}$, $C_{Mg,feed}$, $C_{Na,permeate}$, and $C_{Na,feed}$ are mole concentrations of Li^+, Mg^{2+} and Na^+ in the permeate and feed chambers, respectively.

3. Results and discussion

3.1. Morphology and microstructural study of the LATP phase

The XRD patterns of LATP nanoparticles calcined at temperatures ranging from 500 °C to 950 °C are shown in Fig. 2. The peaks at 2θ = 20°, and 23.5° intensified with increasing calcination temperature because of the enhancement of crystallinity. The crystalline peaks at 2θ = 20°, 23.5°, 28.8°, 31.6°, 35.6°, 46.7°, and 56.5° started to be observed at 600 °C, and finally, intensified diffraction peaks of LATP were observed at 900 °C, which matched the index (JCPDS 35-0754) and previous studies [16,38]. Although no impurity peaks were observed, the peak at 2θ = 15° (found at 650–900°) disappeared at 950 °C, probably because of Li loss, which several studies have reported [39,40]. The choice of sintering temperature for thin film deposition is crucial because it indicates the upper limit to which the calcination temperature can be raised. It is essential to consider that excessively high temperatures can result in Li loss, altering the pathways of Li conduction and subsequently impacting the overall performance of the membrane. Therefore, it is preferable to maintain the sintering temperature at approximately 900 °C to ensure optimal membrane performance during thin film deposition.

The morphologies of LATP nanoparticles synthesized by the sol–gel method are shown in Fig. 3. The average particle sizes are approximately 30 and 100 nm at 700 °C (a) and 850 °C (b), respectively.

3.2. Morphology study of the membrane

The fabrication of thin dense ceramic membranes on porous alumina supports using a sol–gel coating is a complex endeavor that presents significant challenges. Multiple coatings must be applied to achieve a membrane under optimal conditions, and subsequent sintering processes must be performed. One approach to achieving a highly densified structure involves subjecting the membrane to high temperatures exceeding 1000 °C. However, this elevated temperature can often result in the development of substantial cracks and openings within the membrane, which are unacceptable for its intended purpose. The performance of a thin ceramic membrane is largely contingent upon the membrane's continuity. Employing multiple coatings and subsequent sintering processes can contribute to the creation of a continuous, densified ceramic membrane.

To investigate the influence of the coating number, two membranes were fabricated for comparative analysis. At first, a single-coated membrane was prepared by dipping one side of the alumina substrate into the LATP sol for 6 s. After that, the membrane was dried and subsequently sintered at 850 °C. The double-coated membrane was prepared by coating the LATP sol on the single-coated membrane, followed by drying and sintering at the same temperature. The cross-sectional SEM images of single-coated and double-coated membranes are shown in Fig. 4 (a) and (b), respectively.

Based on the obtained cross-sectional images as shown in Fig. 6 of the single- and double-coated membranes, it was determined that the number of coatings notably influences the membrane's structure. The average thickness of the single-coated membrane was measured at 11.58 ± 1.22 μm, while the double-coated membrane exhibited an average thickness of 14.32 ± 1.36 μm. This observation suggests that the second

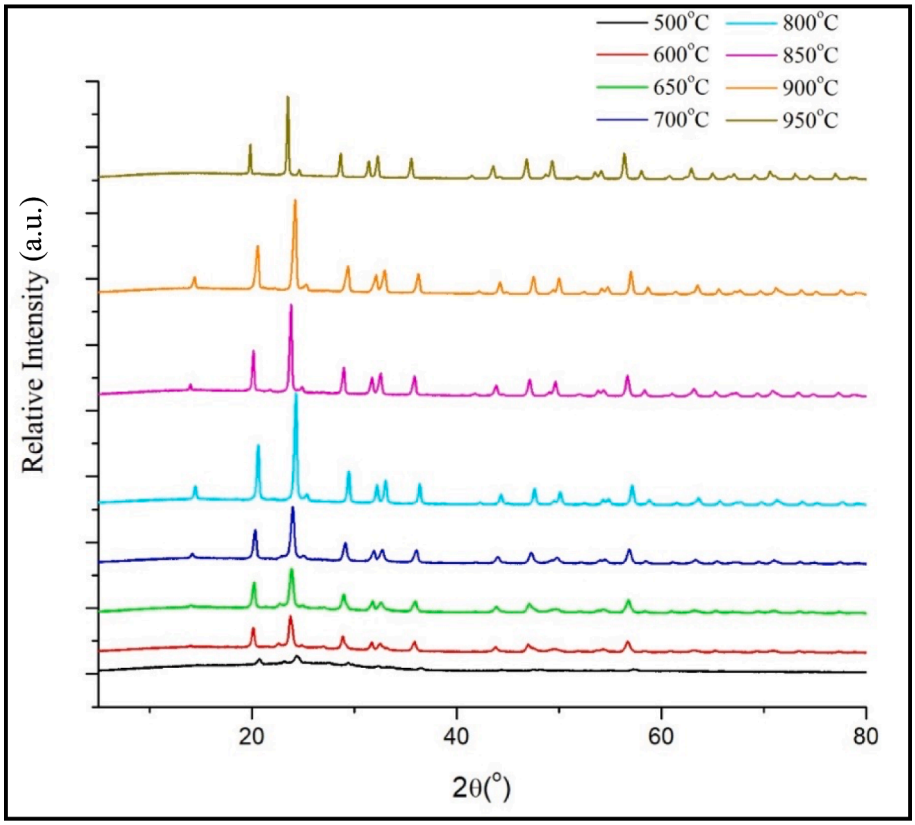

Fig. 2. XRD pattern of LATP at different temperatures.

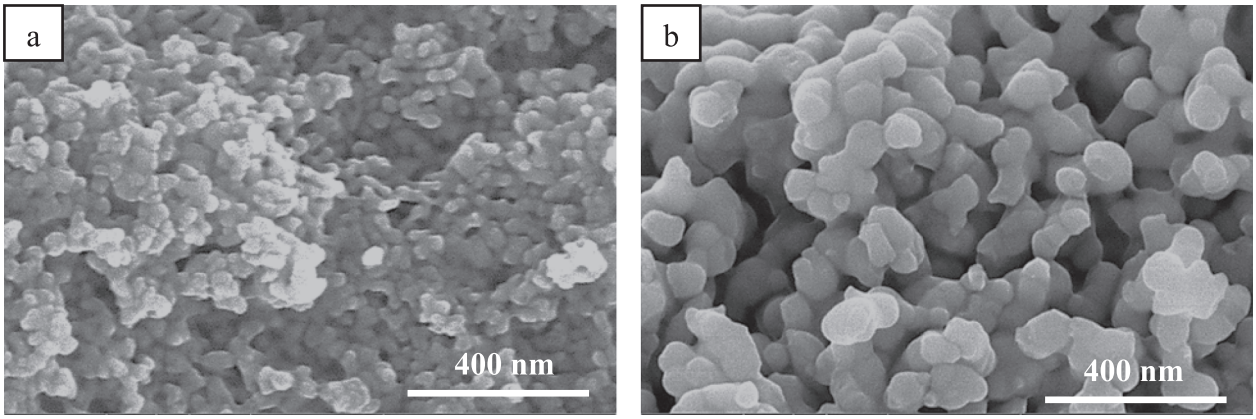

Fig. 3. SEM images of LATP particles sintered at (a) 700 °C and (b) 850 °C.

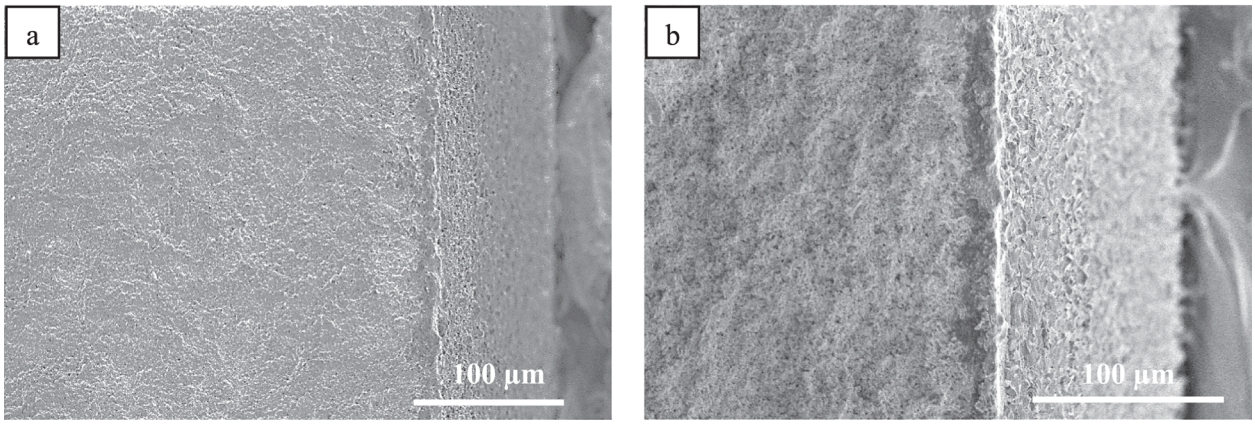

Fig. 4. Cross-sectional SEM images of (a) single- and (b) double-coated membranes.

sol deposition filled surface imperfections within the initial LATP layer. Furthermore, the double-coated membrane displayed a visually more continuous structure compared to the single-coated membrane.

The morphology of the surface and cross-sectional images of the membrane sintered at 850 °C are shown in Fig. 5 (a and b), respectively. The SEM surface image as shown in (a and b) represents that a continuous and crack-free layer of LATP was formed and sufficiently covered the porous alumina substrate. However, the surface images of the two LATP/alumina membranes sintered at 850 °C showed that the surface was not smooth. The membrane surface exhibited an inherent polycrystalline structure characterized by grain boundaries, adversely affecting ion conductivity and consequently impacting the membrane's overall performance. When the sintering temperature was set at 850 °C, inadequate grain growth occurred, leading to incomplete coverage of the membrane surface, the formation of a cavity-like structure, and the observation of pinholes. Such a surface morphology facilitates ion deposition and detrimentally affects the membrane's longevity. Conversely, at 900 °C, the membrane surface was free from pinholes.

3.3. Crystallographic analysis

Crystallographic analysis of the membrane was conducted utilizing a Bruker D8 diffractometer, employing grazing X-ray diffraction to minimize the influence of the substrate on the LATP spectra. The XRD spectrums are displayed in Fig. S2a where one can see that several XRD peaks were found to correspond to the LATP spectra (JCPDS 35-0754). The strong peaks of α-Al_2O_3 (JCPDS 05-0712) resulted from the alumina substrate. Interestingly, the XRD spectrum exhibited the presence of a small amount of impurity TiO_2 in addition to LATP and Alumina. This observation can likely be attributed to the loss of Li for a long time sintering at high temperatures [41,42].

3.4. Membrane performance

In the first stage of performance checking of the LATP/alumina membrane, a double-coated LATP membrane sintered at 850 °C was used as a lithium selective membrane as shown in Fig. 6. The feed solution contained Li^+, Na^+, and Mg^{2+} ions. The operation time was 5 h. The membrane performance largely depends on the quality of the selective layer. The first Mg^{2+} flux was observed after 3 h of operation, which resulted in a high Li/Mg selectivity of 454 ± 227. The change in Li^+ flux was not significant over time. The value was 303 ± 25.89 mmol/m^2/h following a 1 h operation, whereas it was 235 ± 72.7 mmol/m^2/h after 1 h of operation.

On the other hand, the Na^+ flux and Li^+/Na^+ became almost stable after 3 h. The Li^+/Na^+ selectivity was 1.41 ± 0.14 mmol/m^2/h after 5 h. The Li^+/Mg^{2+} selectivity curve significantly plummeted with time, as the Mg^{2+} flux became 2.03 ± 1.32 mmol/h/m^2 from zero flux. The final Li^+/Mg^{2+} selectivity decreased to 11.92 ± 012 after 5 h of operation. This was most likely caused by the electrolyte membrane's surface imperfections, which grew greater over time when a voltage was applied. Moreover, LATP is susceptible to the formation of a mixed conduction layer (MCL). MCL is responsible for the degradation of LATP and eventually decreases the membrane performance with time [43]. The comparable ionic radii of Li^+ and Mg^{2+} are likely another factor contributing to the increased Mg^{2+} permeation.

In the second stage of performance checking of the LATP/Alumina membrane, to determine the effect of the process parameter of the

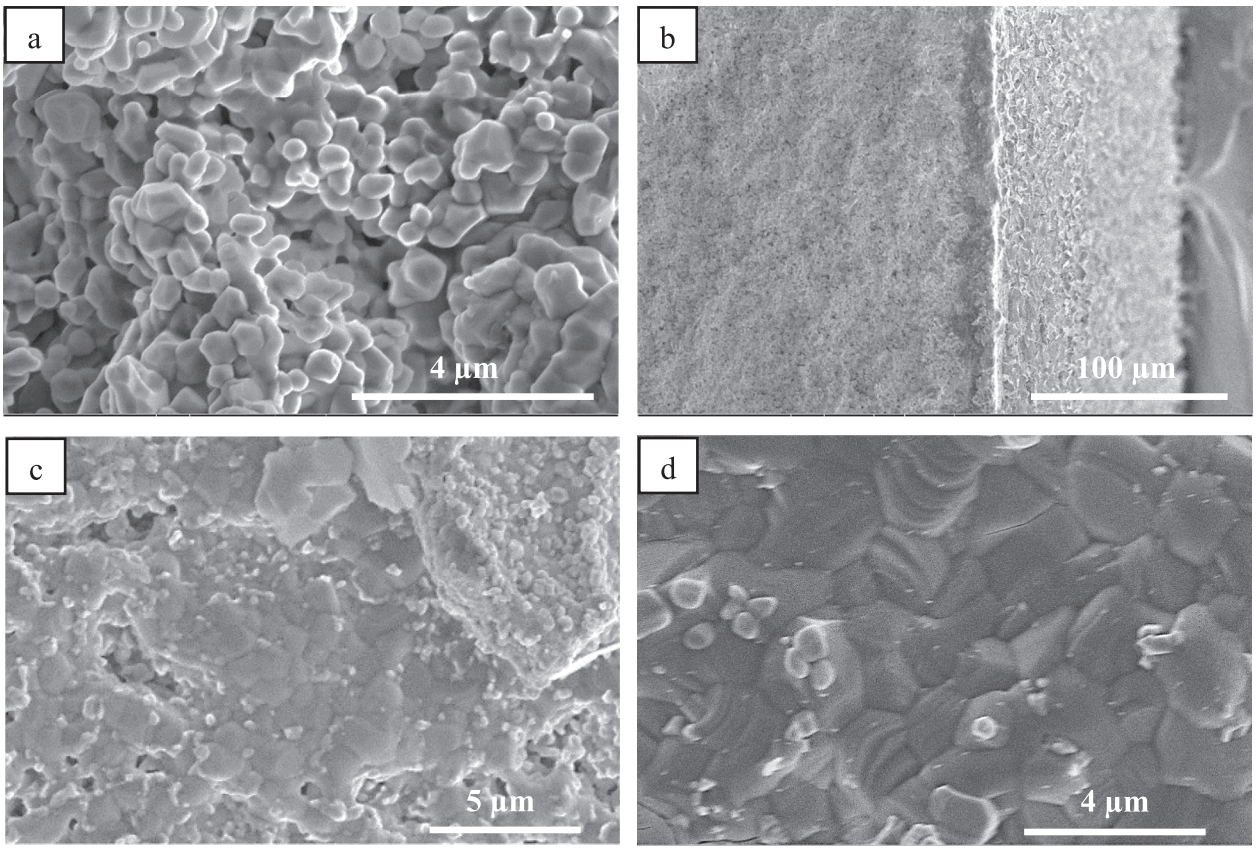

Fig. 5. (a) SEM image of the surface of the porous alumina substrate, (b) cross-sectional SEM image of the LATP/alumina membrane, the surface of the LATP/alumina membrane sintered at (c) 850 °C and (d) 900 °C.

membrane preparation, the membrane was sintered at 800 and 900 °C in addition to 850 °C. Each membrane was coated two times and subsequently sintered. The performance of these three membranes was evaluated using an electrodialysis process (Fig. 7).

The feed solution contained Li^+, Na^+ and Mg^{2+} ions. The operation time was 5 h. The membrane performance largely depends on the quality of the selective layer. The sintering temperature has a significant effect on the performance of the membrane. Although the ion flux was higher for the membrane sintered at 800 °C, the Li^+/Na^+ and Li^+/Mg^{2+} selectivity was lower, probably because of the lower compactness of the membrane caused by the inadequate sintering temperature of 800 °C. A slight improvement was seen in the Mg^{2+} rejection for the membrane sintered at 850 °C. The membrane was able to block Mg^{2+} for 2 h. The membrane with the best Mg^{2+} rejection, sintered at 900 °C, was able to completely reject Mg^{2+} for four hours. The first Mg^{2+} flux was observed after 4 h of operation, which resulted in a high Li/Mg selectivity of 149. The final Li^+/Mg^{2+} selectivity was 33, with the possibility of decreasing more as the curve did not reach an equilibrium value even after 5 h of operation. This implies that the sintering temperature has a significant effect on membrane performance.

There is still a need for further research to comprehend the underlying reasons for the increase in Mg^{2+} flux over time, decreasing the Li^+/Mg^{2+} selectivity. In contrast, the sintering temperature did not exhibit a significant effect on Li^+/Na^+ selectivity. Equilibrium was nearly achieved after 3 h of operation in terms of Na^+ flux and Li^+/Na^+ selectivity.

The obtained membrane sintered at 900°, exhibited an impressive Li^+/Mg^{2+} selectivity of 33, which significantly surpasses the selectivity values of commercial ion-exchange membranes commonly employed in electrodialysis methodology, as depicted in Table 1. This finding substantiates that the enhanced selectivity arises from the presence of the LATP layer, while the alumina layer fulfills the crucial role of providing appropriate support to ensure the membrane's robustness.

3.5. Membrane stability and mechanical strength

For the LATP/alumina membrane to last longer, electrochemical stability preservation is crucial. During the electrodialysis process, the membrane is stacked under a potential difference. Due to electrochemical influence, the intrinsic properties of the membranes can change during the electrodialysis process. The XRD spectra of fresh and used LATP/Alumina double-coated membranes, sintered at 900°, were thus compared in Fig. S2**b** as a measure of the membrane's stability. The characteristic peaks of LATP were unaltered after the operation. The unaltered crystal structure resembles the stability of the membrane even after use.

For the LATP membrane to last longer, it is crucial that its mechanical qualities are retained. A micro-indentation test was performed on the single-coated and double-coated membranes to determine the effect of the coating number. The hardness of the used membrane was also tested to comprehend the mechanical performance of the membranes. The hardness values for the single-coated and double-coated LATP membranes sintered at 850 °C are 48 ± 11.4 and 115 ± 18.9 HV, respectively. The outcome also supports the use of a double coating for increased mechanical strength. The sintering temperature affects the hardness of the LATP coating. Single-coated membranes sintered at 850 °C and 900 °C had hardness values of 48 ± 11.4 and 68 ± 19.56 HV, respectively. After using the hardness, the number of double-coated LATP membranes sintered at 850 °C decreased to 55 ± 10 HV. The probable reason for decreasing the hardness is the accumulation of ions in the surface defects.

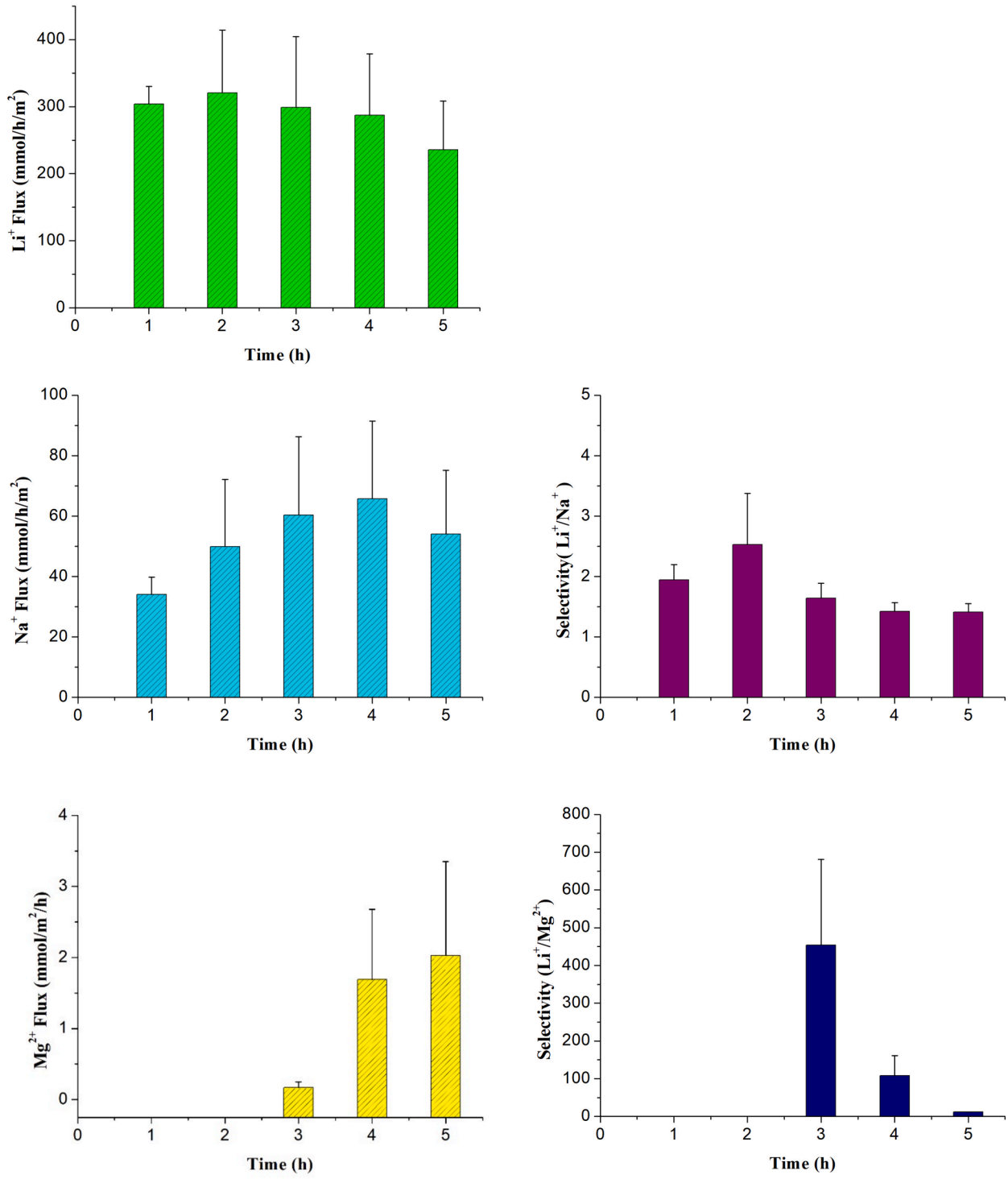

Fig. 6. (a) Li^+, (b) Na^+ and (c) Mg^{2+} ion flux, (d) Li^+/Na^+ selectivity and (e) Li^+/Mg^{2+} selectivity of the double-coated LATP/Alumina membrane sintered at 850 °C.

4. Conclusion

This study developed a LATP/alumina membrane to selectively separate Li^+ from Na^+ and Mg^{2+}. The experimental approach of using sol–gel coating successfully yielded a pure LATP phase and a stable LATP sol, providing a suitable recipe for membrane preparation. By utilizing sol–gel dip coating, a LATP thin film membrane was effectively fabricated on a porous alumina substrate, resulting in a two-layer asymmetric architecture. Notably, a continuous LATP film on the porous support was achieved by carefully controlling the sol solution concentration, the number of coatings, and subsequent sintering and heat treatment cycles, marking the first report of such a fabrication method.

This research investigated the effect of sol coating quantity on the formation of a continuous lithium aluminum titanium phosphate (LATP) membrane on a porous alumina substrate. Additionally, the influence of the sintering temperature employed during membrane preparation on both ion flux and selectivity was clarified. Li^+/Mg^{2+} selectivity was found to be higher for the membrane sintered at a comparatively high temperature. The membrane sintered at 900^OC, effectively blocked Mg^{2+} for 4 h. Nevertheless, selectivity diminishes over time. This finding

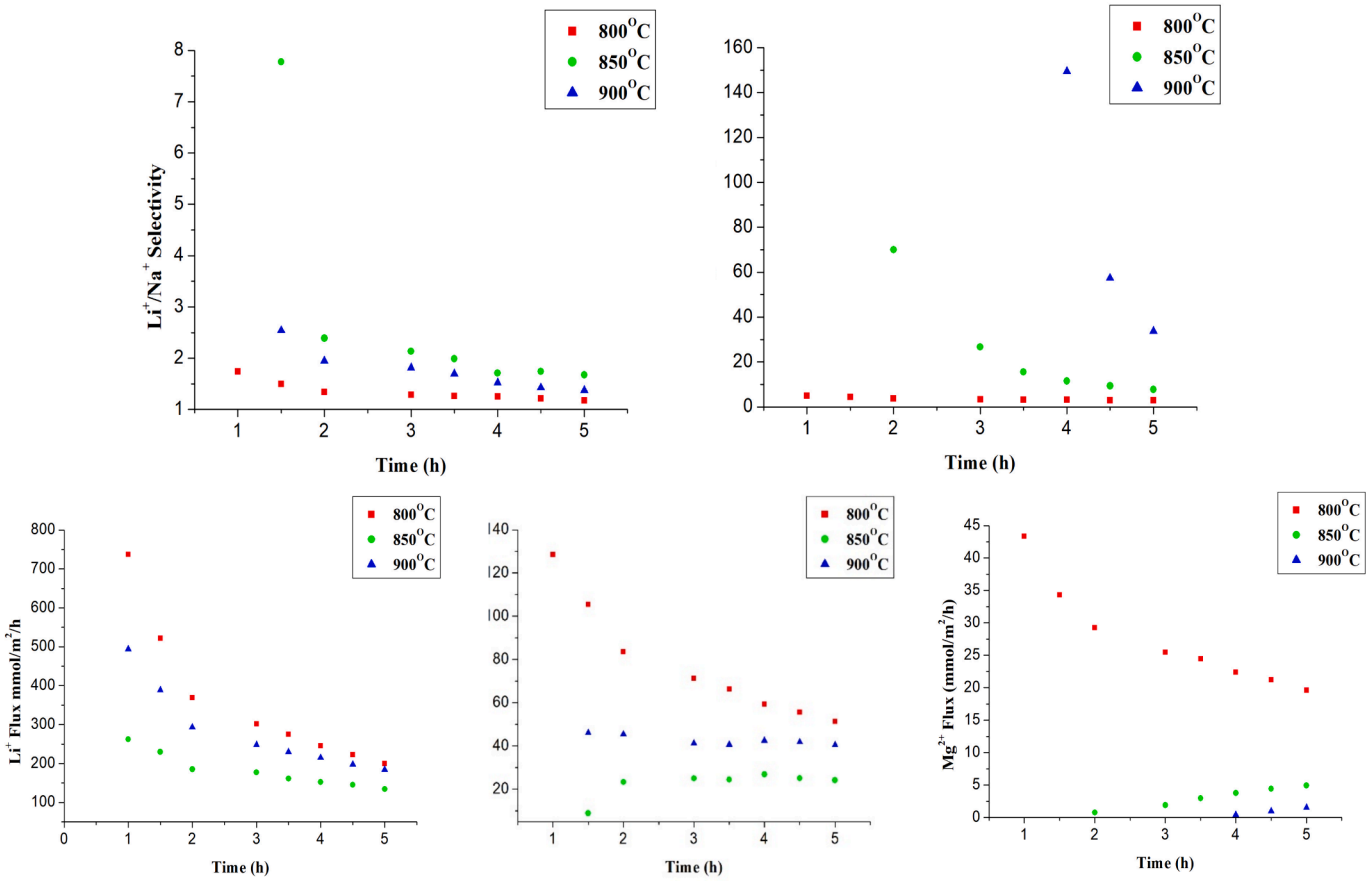

Fig. 7. Comparison of (a) Li^+/Na^+ selectivity, (b) Li^+/Mg^{2+} selectivity, (c) Li^+ flux, (d) Na^+ flux, and (e) Mg^{2+} flux for the LATP/Alumina membrane sintered at 800°, 850° and 900 °C.

Table 1
Comparative study of Li extraction using the electrodialysis method.

Membrane type	Electrical mode	Performance (selectivity)	Ref
Selemion CSO, Selemion ASA	Current concentration, CC = 5.9 A/m2	Li^+/Mg^{2+}= 20.2–33.0	[13]
Selemion CSO, Selemion ASA	Voltage, V = 6.0 V	Li^+/Mg^{2+}=17.9	[44]
Selemion CSO, Selemion ASA	Voltage, V = 12–28 V	Li^+/Mg^{2+}=9.89	[44]
Neosepta CIMS, Neosepta ACS	Voltage, V = 5.0 V	Li^+/Mg^{2+}=20	[45]
Neosepta CIMS Neosepta ACS	Voltage, V = 5.0 V	Li^+/Mg^{2+}=13	[46]
LATP/alumina membrane	Voltage, V = 2.0 V	Li^+/Mg^{2+}=33	This work

highlights the need for developing strategies to sustain Li^+/Mg^{2+} for a longer time, thereby paving the way for future membranes that can enable efficient lithium extraction processes.

CRediT authorship contribution statement

Umma Habiba: Writing – original draft, Methodology, Investigation. **Tawsif Ahmed Siddique:** Methodology. **Islam Md Rizwanul Fattah:** Writing – review & editing. **Shabin Mohammed:** Methodology. **Edward Attenborough:** Methodology. **Quan Lai:** Methodology. **Zhouyou Wang:** Supervision.

Declaration of competing interest

The authors declare that they have no known competing financial interests or personal relationships that could have appeared to influence the work reported in this paper.

Acknowledgment

This work was supported by the Australian Research Council through Huanting Wang's Australian Laureate Fellowship (Project no. FL200100049). The authors acknowledge Prof. Huanting Wang for supervision. The authors acknowledge the Monash Centre for Electron Microscopy, the Monash X-ray platform and Dr. Jiseng Ma for his assistance with grazing X-ray diffraction. The authors also acknowledge Dr. Nhi Sa Nguyen for her contribution to the electrodialysis setup.

Appendix A. Supplementary material

Supplementary data to this article can be found online at https://doi.org/10.1016/j.seppur.2024.128657.

References

[1] L. Talens Peiró, G. Villalba Méndez, R.U. Ayres, Lithium: sources, production, uses, and recovery outlook, JOM 65 (8) (2013) 986–996.
[2] Lithium Prices Have Nearly Doubled In 2022 Amid Insane Commodity Rally. u. finance.yahoo.com/news/lithium-prices-nearly doubled-2022-170000490.html.
[3] B. Swain, Recovery and recycling of lithium: a review, Sep. Purif. Technol. 172 (2017) 388–403.
[4] S. Gmar, A. Chagnes, Recent advances on electrodialysis for the recovery of lithium from primary and secondary resources, Hydrometall. 189 (2019) 105124.

[5] P. Meshram, B. Pandey, T. Mankhand, Extraction of lithium from primary and secondary sources by pretreatment, leaching and separation: a comprehensive review, Hydrometall. 150 (2014) 192–208.
[6] A. Khalil, et al., Lithium recovery from brine: recent developments and challenges, Desalination 528 (2022) 115611.
[7] X. Zhao, et al., Review on the electrochemical extraction of lithium from seawater/brine, J. Electroanal. Chem. 850 (2019) 113389.
[8] A. Somrani, A.H. Hamzaoui, M. Pontie, Study on lithium separation from salt lake brines by nanofiltration (NF) and low pressure reverse osmosis (LPRO), Desalination 317 (2013) 184–192.
[9] X. Wen, et al., Preliminary study on recovering lithium chloride from lithium-containing waters by nanofiltration, Sep. Purif. Technol. 49 (3) (2006) 230–236.
[10] A. Siekierka, et al., Electro-driven materials and processes for lithium recovery—a review, Membranes 12 (3) (2022) 343.
[11] H. Strathmann, Electrodialysis, a mature technology with a multitude of new applications, Desalination 264 (3) (2010) 268–288.
[12] M. Mulder, J. Mulder, Basic Principles of Membrane Technology, Springer Science & Business Media, 1996.
[13] X.-Y. Nie, et al., Ion-fractionation of lithium ions from magnesium ions by electrodialysis using monovalent selective ion-exchange membranes, Desalination 403 (2017) 128–135.
[14] T.M. Lim, M. Ulaganathan, Q. Yan, Advances in membrane and stack design of redox flow batteries (RFBs) for medium-and large-scale energy storage. InAdvances in Batteries for Medium and Large-Scale Energy Storage, Woodhead Publishing, 2015, pp. 477–507.
[15] Xingyi Shi, et al., Polymer electrolyte membranes for vanadium redox flow batteries: fundamentals and applications, Progress in Energy and Combustion Science 85 (2021) 100926.
[16] S. Takase, et al., Sol–gel processing of Li 1.5 Al 0.5 Ti 1.5 (PO 4) 3 solid electrolyte thin films via polymeric complex precursor, J. Sol-Gel Sci. Technol. 79 (3) (2016) 564–572.
[17] F. Zheng, et al., Review on solid electrolytes for all-solid-state lithium-ion batteries, J. Power Sources 389 (2018) 198–213.
[18] J.W. Fergus, Ceramic and polymeric solid electrolytes for lithium-ion batteries, J. Power Sources 195 (15) (2010) 4554–4569.
[19] H. Duan, et al., Stability of garnet-type Li ion conductors: an overview, Solid State Ion. 318 (2018) 45–53.
[20] Y. Li, et al., Ionic distribution and conductivity in lithium garnet Li7La3Zr2O12, J. Power Sources 209 (2012) 278–281.
[21] Y. Zhang, et al., Field assisted sintering of dense Al-substituted cubic phase Li7La3Zr2O12 solid electrolytes, J. Power Sources 268 (2014) 960–964.
[22] T. Thompson, et al., Electrochemical window of the Li-ion solid electrolyte Li7La3Zr2O12, ACS Energy Lett. 2 (2) (2017) 462–468.
[23] M. Monchak, et al., Lithium diffusion pathway in Li1.3Al0.3Ti1.7(PO4)3 (LATP) superionic conductor, Inorg. Chem. 55 (6) (2016) 2941–2945.
[24] M. Biswas, P.-C. Su, Chemical Solution Deposition Technique of Thin-Film Ceramic Electrolytes for Solid Oxide Fuel Cells. Modern Technologies for Creating the Thin-film Systems and Coatings, 2017: p. 319.
[25] L. Huang et al., Electrochemical properties of Li1. 4Al0. 4Ti1. 6 (PO4) 3 synthesized by a coprecipitation method, J. Power Sources 196(16) (2011) 6943-6946.
[26] L.L. Hench, J.K. West, The sol-gel process, Chem. Rev. 90 (1) (1990) 33–72.
[27] L. Znaidi, Sol–gel-deposited ZnO thin films: a review, Mater. Sci. Eng. B 174 (1–3) (2010) 18–30.
[28] J.-H. Lee, B.-O. Park, Transparent conducting ZnO: Al, In and Sn thin films deposited by the sol–gel method, Thin Solid Films 426 (1–2) (2003) 94–99.
[29] R. Asri, et al., A review of hydroxyapatite-based coating techniques: Sol–gel and electrochemical depositions on biocompatible metals, J. Mech. Behav. Biomed. Mater. 57 (2016) 95–108.
[30] M. Sahal, et al., Structural, electrical and optical properties of ZnO thin films deposited by sol–gel method, Microelectron. J. 39 (12) (2008) 1425–1428.
[31] P. Jia, et al., Pechini sol–gel deposition and luminescence properties of Y3Al5−xGaxO12: Ln3+ (Ln3+= Eu3+, Ce3+, Tb3+; 0≤ x≤ 5) thin films, Thin Solid Films 483 (1–2) (2005) 122–129.
[32] T.O.L. Sunde, T. Grande, M.-A. Einarsrud, Modified pechini synthesis of oxide powders and thin films. Handbook of Sol-Gel Science and Technology, 2016.
[33] V. Agarwal, M. Liu, Preparation of barium cerate-based thin films using a modified Pechini process, J. Mater. Sci. 32 (3) (1997) 619–625.
[34] T.N. Soitah, et al., Properties of Bi2O3 thin films prepared via a modified Pechini route, Curr. Appl Phys. 10 (6) (2010) 1372–1377.
[35] R.W. Schwartz, Chemical solution deposition of perovskite thin films, Chem. Mater. 9 (11) (1997) 2325–2340.
[36] L. Dimesso, Pechini processes: an alternate approach of the sol–gel method, preparation, properties, and applications, Handbook Sol-Gel Sci. Technol. 2 (2016) 1–22.
[37] P.-Y. Yen, et al., Optimization of sintering process on Li1+ xAlxTi2-x (PO4) 3 solid electrolytes for all-solid-state lithium-ion batteries, Ceram. Int. 46 (12) (2020) 20529–20536.
[38] S. Duluard et al., Lithium conducting solid electrolyte Li1. 3Al0. 3Ti1. 7 (PO4) 3 obtained via solution chemistry, J. Euro. Ceram. Soc. 33(6) (2013) 1145-1153.
[39] Z. Li, X. Zhao, Influence of excess lithium and sintering on the conductivity of Li 1. 3 Al 0. 3 Ti 1. 7 (PO4) 3. Funct. Mater. Lett. 12(4) (2019) 1950047.
[40] K. Waetzig, C. Heubner, M. Kusnezoff, Reduced sintering temperatures of Li+ conductive Li1. 3Al0. 3Ti1. 7 (PO4) 3 ceramics, Crystals 10(5) (2020) 408.
[41] A. Mohammadzadeh, et al., in: Mechanical Engineering of Solid Oxide Fuel Cell Systems: Geometric Design, Mechanical Configuration, and Thermal Analysis, Academic Press, 2020, pp. 85–130.
[42] M. Kimpa, et al., Sol-Gel synthesis and electrical characterization of Li1+ xAlxTi2-x (PO4) 3 solid electrolytes, J. Sci. Technol. 9 (3) (2017) 106–112.
[43] P. Hartmann, et al., Degradation of NASICON-type materials in contact with lithium metal: formation of mixed conducting interphases (MCI) on solid electrolytes, J. Phys. Chem. C 117 (41) (2013) 21064–21074.
[44] X.Y. Nie, et al., Further investigation into lithium recovery from salt lake brines with different feed characteristics by electrodialysis, J. Membr. Sci. 530 (2017) 185–191.
[45] Q.B. Chen, et al., Development of recovering lithium from brines by selective-electrodialysis: Effect of coexisting cations on the migration of lithium, J. Membr. Sci. 548 (2018) 408–420.
[46] Z.Y. Ji, et al., Preliminary study on recovering lithium from high Mg2+/Li+ ratio brines by electrodialysis, Sep. Purif. Technol. 172 (2017) 168–177.